

How oscillations in SIRS epidemic models are affected by the distribution of immunity times

Daniel Henrik Nevermann and Claudius Gros

Models for resident infectious diseases, like the SIRS model, may settle into an endemic state with constant numbers of susceptible (S), infected (I) and recovered (R) individuals, where recovered individuals attain a temporary immunity to reinfection. For many infectious pathogens, infection dynamics may also show periodic outbreaks corresponding to a limit cycle in phase space. One way to reproduce oscillations in SIRS models is to include a non-exponential dwell-time distribution in the recovered state. Here, we study a SIRS model with a step-function-like kernel for the immunity time, mapping out the model's full phase diagram. Using the kernel series framework, we are able to identify the onset of periodic outbreaks when successively broadening the step-width. We further investigate the shape of the outbreaks, finding that broader steps cause more sinusoidal oscillations while more uniform immunity time distributions are related to sharper outbreaks occurring after extended periods of low infection activity.

Our main results concern recovery distributions characterized by a single dominant timescale. We also consider recovery distributions with two timescales, which may be observed when two or more distinct recovery processes co-exist. Surprisingly, two qualitatively different limit cycles are found to be stable in this case, with only one of the two limit cycles emerging via a standard supercritical Hopf bifurcation.

1. Introduction

The COVID-19 pandemic showed that it is important to understand infection dynamics from two distinct viewpoints. Firstly it is important to examine and understand a given active outbreak, secondly a thorough understanding of the general theory is necessary, with the latter being the topic here. Today, the Corona virus resides in an endemic state

that is periodically disrupted by seasonal fluctuations or sudden outbreaks followed by periods of less viral activity, a behavior that is characteristic also for other resident infectious diseases, like influenza, measles and pertussis [15].

Synchronization phenomena in the form of oscillatory infection dynamics may be caused by a number of different interfering factors. External drivers include seasonality [14] or behavioral changes, potentially imposed by disease prevention measures [6]. Other factors can be the nature of the network of contacts [13], travel [5] and even stochastic effects [1]. Taking a modeling point of view, the present study aims to improve the understanding of the origins of oscillations as arising from an endogenous cause, namely from the distribution of immunity times when people are recovering from a disease.

Individuals in populations exposed to infective pathogens typically pass through different stages, usually modeled via population subclasses. Non-infected individuals remain in the susceptible class S until a contagion event happens, which moves the individual into the infected class I . Recovering from the disease, an individual usually builds-up a temporary immunity, which puts the individual into the class of recovered R .¹ Once immunity decayed, the individual returns to be susceptible, which completes the cycle. The standard SIRS model has the form

$$\begin{aligned} \dot{I} &= \beta IS - \rho I \\ \dot{R} &= \rho I - \gamma R \end{aligned}, \quad 1 = S + I + R, \quad (1)$$

where β is the infection rate per individual, ρ is the recovery rate and γ is the immunity-fade rate. This formulation assumes exponential decay from a given to a subsequent compartment, where the inverse of the decay rates define characteristic dwell times. While SIRS models of the form (1) capture damped oscillations towards a stationary state, the endemic state, oscillatory states and/or states with periodic outbreaks cannot be modeled.

Recently, several modifications to the standard SIRS model have been proposed, with some versions able to produce sustained oscillations, typically when time delays are present. In [19] the authors try to incorporate human behavior by including mitigation effects driven by perceived hazards, as characterized through past infection numbers. Sustained oscillations are obtained further-on when including time delays in the dwell-time distribution in the recovered compartment. Previous works considering non-exponential immunity time distributions [3, 7] find that oscillations appear depending on the specific choice of the delay kernel. If the kernel is given in terms of Erlang distributions,² the kernel series framework [16] can be applied to rewrite the time-delay model in terms of an extended set of ordinary differential equations. Similar approaches have been considered in the past, see [12]. Alternatively, the effect of non-trivial dwell-time distributions in the infected compartment has been examined, e.g. as in [8].

In this contribution, we consider models with arbitrary immunity-time distributions, compare [10]. Of special interest will be immunity kernels having the form of a step func-

¹Individuals in the R class by be considered to be either ‘recovered’, or ‘recovering’, depending on the terminology used. Note that infected (ill) individuals are considered to be immune too.

²Erlang distributions are of the form $\lambda^n x^{n-1} e^{-\lambda x} / (n-1)!$, with positive support, $x \geq 0$. The parameters are $\lambda > 0$ (real) and $n > 1$ (integer).

tion, which we denote block delay kernels, and in particular broadened step functions, here denoted soft steps, that allow to interpolate smoothly between the classical SIRS model (1), for which immunity is distributed exponentially, and the situation where immunity is identical for all individuals. In the latter case, a mapping to the corresponding discrete-time model is possible. We find that stable limit cycles describing non-uniform infectious dynamics emerge via a supercritical Hopf bifurcation [9], when either increasing average immunity times and/or decreasing the width of the corresponding smooth step.

The paper is organized as follows. In Sec. 2 we discuss the SIRS model used in our analyses, featuring a soft step delay distribution for the time individuals retain immunity. Before presenting the model we start with an outline of the kernel series framework and a SIRS model with general immunity time kernel. Afterwards, in Sec. 3, we present our results for the onset and the shape of periodic outbreaks when varying the step width. Finally, we discuss our results in Sec. 4. In the supplementary material, Sec. A, we further present results for a model with two timescales in the recovery distribution.

2. Methods

By applying the kernel series framework to a generalized SIRS model with arbitrary immunity time kernel we aim to systematically study the effects of broadened memory kernels. In particular, we will focus on step-function-like kernels we denote block delay kernels. We start with a brief review of the kernel series framework. For a comprehensive discussion see [16], or literature on the linear chain trick, e.g. [12, 11]. Afterwards, we present a generalized SIRS model and specify to block delay kernels and soft steps.

2.1. Kernel series framework

Using the kernel series framework, delay differential equations with distributed time delays can be translated to a higher dimensional system of ordinary differential equations, granted the time delay kernel is given as a superposition of Erlang kernels. The latter is however not a limitation, given that a general delay kernel may be expanded in terms of Erlang functions [2, 16]. Consider exemplarily the simple case of a one-dimensional system with a time delay distributed according to a single Erlang kernel, denoted here as $K_m^{(N,T)}$,

$$\dot{x}(t) = F(x(t), x_T(t)), \quad x_T(t) = \int_0^\infty x(t - \tau) K_N^{(N,T)}(\tau) d\tau, \quad (2)$$

where the Erlang distribution is defined as

$$K_m^{(N,T)} = \frac{N^m \tau^{m-1} e^{-N\tau/T}}{(m-1)! T^m}, \quad m, N \in \mathbb{N}. \quad (3)$$

In (2), the flow is given by a generic non-linear function $F = F(x, x_T)$, where $x_T = x_T(t)$ is the delay term. Using the kernel series framework, one can recast (2) exactly to the

following $(N + 1)$ -dimensional system of ordinary differential equations:

$$\begin{aligned} \dot{x}(t) &= F(x(t), x_N(t)) \\ \dot{x}_1(t) &= \frac{N}{T}(x(t) - x_1(t)) \\ \dot{x}_m(t) &= \frac{N}{T}(x_{m-1}(t) - x_m(t)), \quad m = 2, \dots, N, \end{aligned} \quad (4)$$

where we introduced a set of auxiliary variables

$$x_m(t) = \int_0^\infty x(t - \tau) K_m^{(N,T)}(\tau) d\tau, \quad m = 1, \dots, N. \quad (5)$$

Since Erlang kernels converge to δ -peaks,

$$\lim_{N \rightarrow \infty} K_N^{(N,T)}(t) = \delta(t - T),$$

the distributed delay included in (2) will converge to a fixed time delay, $x_T = x(t - T)$, in the limit $N \rightarrow \infty$, viz when the dimensionality of the corresponding ODE system (4) diverges. Of interest is also the variance of the Erlang kernel $K_N^{(N,T)}$, which is related to N through

$$\sigma^2 = \frac{T^2}{N}. \quad (6)$$

Thus, by varying N , the kernel series framework can be used as a handy mathematical tool to investigate the response of a system to a broadened memory kernel. An illustration is given in Fig. 1 (b).

2.2. General immunity time kernel

In the standard SIRS model (1) the duration of immunity in a population is assumed to follow an exponential distribution. Generalizing to a generic dwell-time distribution in the recovered compartment leads to

$$\begin{aligned} \dot{I} &= \beta I(1 - I - R) - \rho I \\ R &= \rho \int_0^\infty I(t - \tau) K(\tau) d\tau \quad 1 = S + I + R, \end{aligned} \quad (7)$$

including a distributed time delay with an arbitrary delay kernel $K(t)$. As expected, the original SIRS model (1) is recovered when using an exponential immunity time kernel $K(t) = \gamma \exp(-\gamma t)$ in (7).

In order to apply the kernel series framework, one expands the kernel $K(t)$ in terms of Erlang kernels, which is generally possible, see [2, 16]. For simplicity, we restrict ourselves here to the case that the expansion involves only Erlang kernels with fixed N and T ,

$$K(t) = \frac{T}{N} \sum_{m=1}^N c_m K_m^{(N,T)}(t), \quad (8)$$

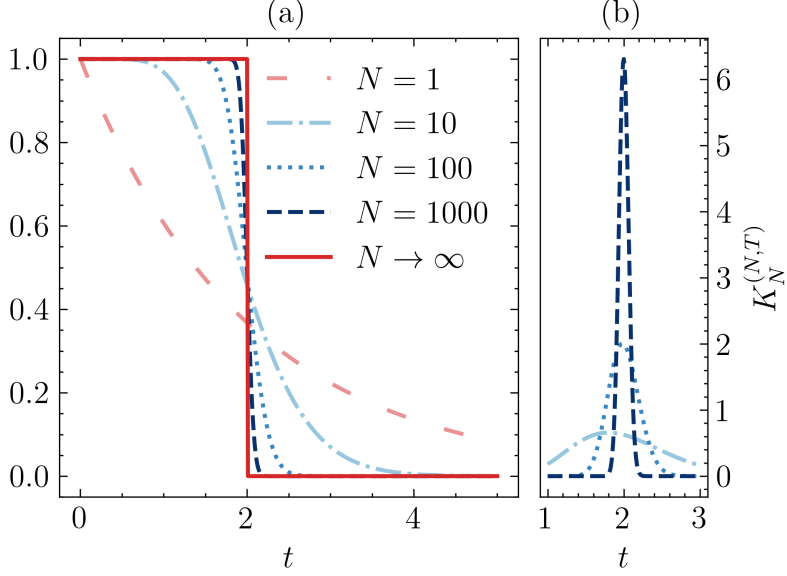


Figure 1: For $T = 2$, an illustration of the step-function kernel defined in (10) in **(a)**. Changing N , allows to interpolate between a block delay kernel ($N \rightarrow \infty$), presenting the limiting case of a discontinuous step function, and an exponential kernel ($N = 1$). **(b)** The step widths are determined by the standard derivative (11), given by the widths of Erlang distribution $K_N^{(N,T)}$, as defined in (3). Therefore, step widths are $\propto 1/\sqrt{N}$, see (6).

where the prefactor is chosen such that $\lim_{t \rightarrow 0} K(t) = 1$. In analogy to (5), we define a series of auxiliary compartments for recovering individuals,

$$R_m = \frac{\rho T}{N} \int_0^\infty I(t - \tau) K_m^{(N,T)}(\tau) d\tau, \quad m = 1, \dots, N,$$

Trivially, computing the c_m -weighted sum of the auxiliary compartments yields the total recovered compartment

$$R = \sum_{m=1}^N c_m R_m.$$

Inserting the ansatz (8) into (7) gives the SIRS model

$$\begin{aligned} \dot{I} &= \beta I \left(1 - I - \sum_{m=1}^N c_m R_m \right) - \rho I \\ \dot{R}_1 &= \rho I - \frac{N}{T} R_1 \\ \dot{R}_m &= \frac{N}{T} (R_{m-1} - R_m) \quad m = 2, \dots, N, \end{aligned} \tag{9}$$

which constitutes the basis of our investigations.

2.3. Smooth step kernels

Specifying the expansion coefficients c_m in (9), distinct immunity-time kernels are generated. A basic choice is $c_m = 1$, which produces immunity distributions describing broadened step functions, we here denote *soft steps*

$$K(t) = \Theta_N^{(T)}(t) = \frac{T}{N} \sum_{m=1}^N K_m^{(N,T)}(t) \xrightarrow{N \rightarrow \infty} \begin{cases} 1, & \text{for } 0 \leq t \leq T \\ 0, & \text{else} \end{cases}, \quad (10)$$

where T defines the location of the step and the parameter N governs the step width, smoothly transitioning between two extremes: a discontinuous step function, we refer to as a *block delay kernel*, as $N \rightarrow \infty$, and an exponential distribution as $N \rightarrow 1$. The kernels are illustrated in Fig. 1 (a). From the derivative,

$$\frac{d\Theta_N^{(T)}}{dt} = -K_N^{(N,T)}(t) < 0, \quad (11)$$

one sees that the soft step kernels decrease strictly monotonic, and that the width of the step is given by the standard deviation of the highest order Erlang kernel in the series, which is $\propto 1/\sqrt{N}$, see (6). The respective Erlang kernels are depicted in Fig. 1 (b).

For the above choice of the expansion coefficients, $c_m = 1$, after application of the kernel series framework, we find that the corresponding SIRS model reads

$$\begin{aligned} \dot{I} &= \beta I \left(1 - I - \sum_{m=1}^N R_m \right) - \rho I \\ \dot{R}_1 &= \rho I - \frac{N}{T} R_1 \\ \dot{R}_m &= \frac{N}{T} (R_{m-1} - R_m), \end{aligned} \quad (12)$$

which is derived from (9). The SIRS model (12) was previously studied in [10]. We here enrich the studies on this model by numerically answering a similar question previously posed in [7], namely the onset of periodic outbreaks when broadening the step of a soft step kernel for the time of immunity and furthermore studying the shape of the periodic outbreaks.

3. Phase Diagram

Using the SIRS model (12) with a step-function-like kernel we study the impact of soft step immunity kernels onto the onset and the shape of periodic outbreaks, where we apply the kernel series framework and therein the order parameter N to interpolate between an exponential kernel ($N \rightarrow 1$) and a block delay kernel ($N \rightarrow \infty$).

3.1. Onset of periodic outbreaks

The (non-oscillatory) endemic state of the model is found at the fixpoint, i.e. at the root of the flow equations in (12). Solving the system of equations yields

$$I_{\text{end}} = \frac{\beta - \rho}{\beta(T\rho + 1)} .$$

As the width of the step function narrows, systematically controlled by increasing the order parameter N , the system undergoes a supercritical Hopf bifurcation, destabilizing the endemic state I_{end} and thereby giving rise to sustained oscillations. Hence, the onset of periodic outbreaks coincides with the Hopf bifurcation point, which is defined as the root of the maximal eigenvalue's real part, $\text{Re}(\lambda_{\text{max}})$, of the system Jacobian evaluated at I_{end} ,

$$\mathbf{J}|_{I_{\text{end}}} = \begin{pmatrix} \frac{\rho - \beta}{T\rho + 1} & \dots & & & \\ \rho & -\frac{N}{T} & & & \\ & \frac{N}{T} & -\frac{N}{T} & & \\ & & \ddots & \ddots & \\ & & & \ddots & \ddots \end{pmatrix} .$$

In the following, for our numerical studies, we use the fixed parameter values $\beta = 2$ and $\rho = 1$ therefore assuming a basic reproduction number $R_0 = 2$, which is a realistic figure for virus endemics such as influenza [4].

In Fig. 2 we show results for the onset of periodic outbreaks. Periodic outbreaks can only appear in a subset of the full parameter landscape (N, T) , as indicated by the bifurcation diagram in Fig. 2 (a). The step width necessary to observe periodic outbreaks is strongly influenced by the immunity time, imposed through the parameter T in the kernel. For larger immunity times, oscillations already occur at relatively wide steps, compare Fig. 1 (a). However, as the immunity time approaches the Hopf bifurcation curve, much narrower step widths are necessary for the emergence of endemic oscillations, see Fig. 2 (b).

3.2. Shape of periodic outbreaks

The impact of soft step delay kernels extends beyond the appearance of periodic outbreaks. The shape of the periodic outbreaks also changes with the diversity of time scales at which individuals loose immunity, given by the step width of the soft step (10). Notably, we find that softer steps render the periodic oscillations more sinusoidal while a narrower step width induces sharp outbreaks separated by extended time spans where the disease is out of season. These tendencies can be observed in Fig. 3. As a compounded measure for the shape of the periodic outbreaks we employ the skewness μ_3 of the time series. For narrower step widths, the probability density associated with the time series clearly shows increasingly positive skew, see Fig. 3 (a). With increasing N , that is decreasing step widths, the skewness quickly approaches an upper bound given by the skewness of the time series in the limit $N \rightarrow \infty$. We show that the relative deviation of the finite N skewness from its upper bound scales roughly as a power-law.

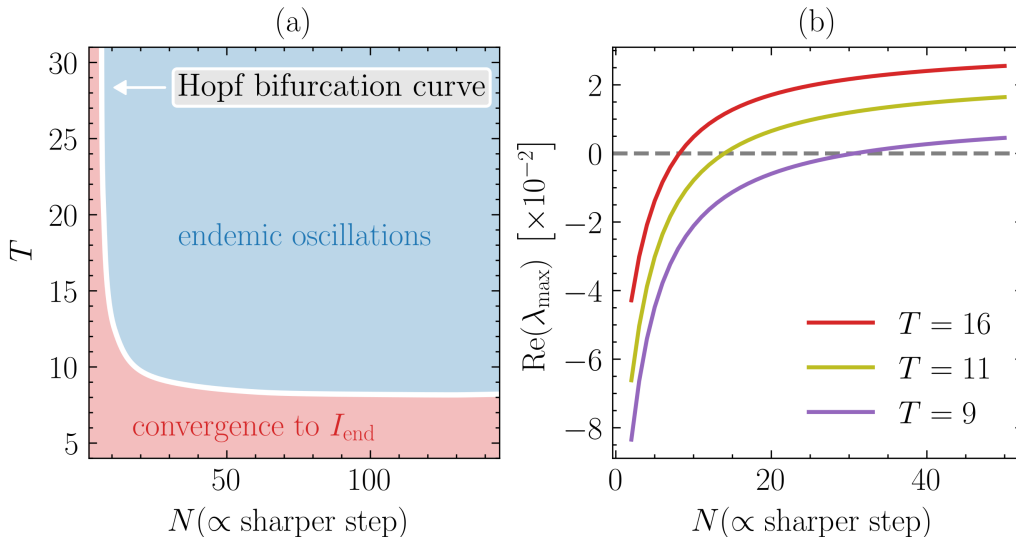


Figure 2: Onset of periodic outbreaks characterized through a Hopf bifurcation point, which occurs at the root of the maximal eigenvalue’s real part of the system Jacobian evaluated at I_{end} , $\text{Re}(\lambda_{\text{max}})$. Positive values correspond to periodic outbreaks. In (a) we show the region of the parameter landscape (N, T) , where periodic outbreaks occur for $\beta = 2$ and $\rho = 1$ shaded in blue, while the system converges to the endemic state for parameters in the red-shaded region. Selected horizontal cross-sections for $T = 9, 11, 16$ are given in (b).

Similar scaling of relative deviations for various dynamical quantities in the kernel series framework was previously observed in [16].

4. Discussion

Oscillations are an omnipresent feature of epidemic dynamics. A comprehensive understanding is important for policymakers as well as epidemic modelers, in particular regarding preventive measures. In the present work we investigated oscillations in time-delay SIRS models using a recently developed method, the kernel series framework [16], which is applicable to arbitrary immunity time kernels, viz to any type of dynamics leading to the successive loss of immunity in the recovered population. A particular focus of our study concerns the relative influence of two types of immunity dynamics, which may be lost either progressively or rather abruptly, as described by immunity kernels having the form of a broadened step function, here denoted soft steps. We were able to identify the onset of oscillations with respect to the softness of the step in the immunity time kernel and identify a relation between the step width with the shape of the periodic outbreaks.

The standard SIRS model (1) takes a mean-field approach by including an exponentially distributed decay of immunity in the population, where the inverse of the decay

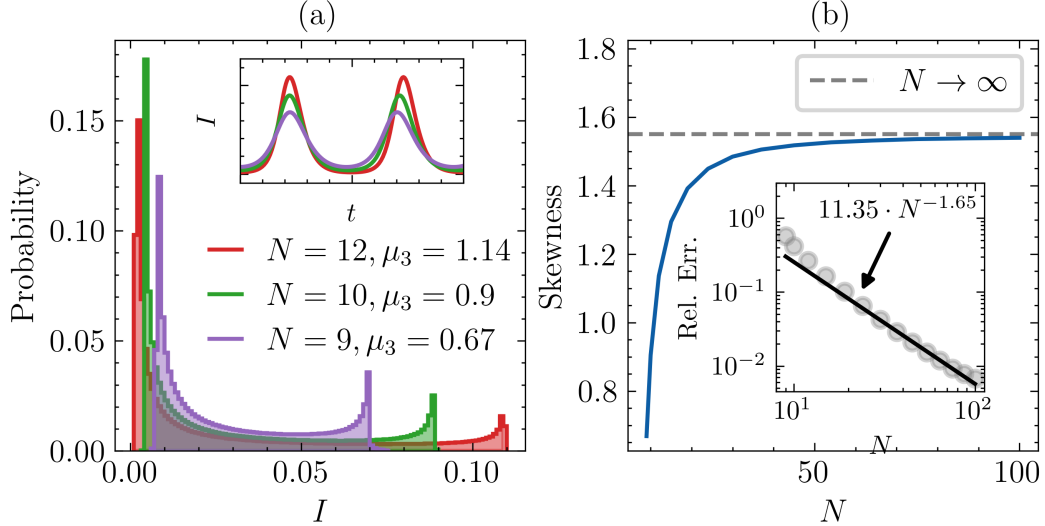


Figure 3: In **(a)**, probability densities associated to the time series in the SIRS model (12) with $\beta = 2$ and $\rho = 1$ for different values of N , viz different step widths of the soft step kernel (10), along with the respective time series presented in the inset. The time constant in the kernels is kept at $T = 16$. Softer steps, i.e. smaller figures of N , imply more sinusoidal periodic outbreaks and therefore smaller positive skew. **(b)** The skewness converges to the value found in the time-delay system at $N \rightarrow \infty$, where the relative error to the system with (discontinuous) block delay kernel scales roughly as a power-law $\propto N^{-1.65}$.

constant $1/\gamma$ defines the average time until an individual loses immunity. An alternative are discontinuous delay kernels (with infinitely sharp steps), which describes the case where every individual is immune for exactly the same period T . This limit, however, neglects population diversities. The kernel series framework [16] provides a convenient mathematical tool to probe the interpolation between the two limiting cases by investigating the effect of smoothed block kernels. Adding a second smoothed step to the block delay kernel (see Sec. A) extends the model to a second type of population diversity, namely in terms of two characteristic immunity times. Epidemiologically, one can imagine dividing the population into subgroups based on factors such as pre-existing conditions (e.g., diabetes) or demographic factors (e.g., age or gender). That being said, we acknowledge that a realistic modelling of disease dynamics from which policy implications may be drawn would require more complex immunity time kernels, potentially tailored to specific diseases. For this direction, further research is required.

Despite stylized assumptions for the immunity time kernels, the reported implications of smoothed kernels onto shape and presence of periodic outbreaks could be important in the crafting of infection prevention plans. The presence of periodic outbreaks might require timed countermeasures such as vaccination campaigns, lockdowns or behavioral changes. Furthermore, different shapes of outbreaks might demand tailored prevention strategies, where e.g. sudden severe outbreaks could require more directed countermea-

tures than sinusoidal oscillations. Our results highlight the importance of considering immunity time kernels in epidemic forecasting.

Taking the timescale of the constant T in the immunity time kernel, which is given in units of the mean dwell time in the infected state, $\langle T_{\text{infected}} \rangle = 1/\rho$, allows to place oscillation periods and characteristic time delays into context. For a block delay kernel, we find that oscillations appear for immunity times $T \approx 8 \cdot \langle T_{\text{infected}} \rangle$ (see Fig. 2 and [17]). For a two-step kernel the onset of oscillations occurs only at significantly larger values of T .

Contrary to the single-step model, we found multi-stability in the two-step model, see Sec. A, which implies a strong dependence on initial conditions. Similar multistabilities in time-delay SIRS models were found previously, e.g. in [3]. If the system resides close to its fixpoint it will either converge back to the fixpoint or show mild periodic outbreaks. For different initial conditions, such as a patient zero in a susceptible population, the system asymptotically shows severe periodic outbreaks affecting up to $\approx 80\%$ of the population. The origins of endemic oscillations not induced through a Hopf bifurcation as well as potentially similar limit cycles in models with more complex immunity kernels, such as three-step kernels, and their epidemiological interpretation are subject to future research. For policymakers, the potential existence of more than one stable epidemic states would have sever implications. Applying a suitable chock therapy, like kick control [18], may be considered, with the goal 'to kick' the system from an unfavorable attractor into a comparatively more benign epidemic state.

References

- [1] Juan Pablo Aparicio and Hernán Gustavo Solari. “Sustained oscillations in stochastic systems”. In: *Mathematical biosciences* 169.1 (2001), pp. 15–25.
- [2] Joel Bergé et al. “Exponential shapelets: basis functions for data analysis of isolated features”. en. In: *Monthly Notices of the Royal Astronomical Society* 486.1 (June 2019), pp. 544–559. ISSN: 0035-8711, 1365-2966. DOI: [10.1093/mnras/stz787](https://doi.org/10.1093/mnras/stz787).
- [3] Michael Bestehorn et al. “Simple model of epidemic dynamics with memory effects”. en. In: *Physical Review E* 105.2 (Feb. 2022), p. 024205. ISSN: 2470-0045, 2470-0053. DOI: [10.1103/PhysRevE.105.024205](https://doi.org/10.1103/PhysRevE.105.024205).
- [4] Matthew Biggerstaff et al. “Estimates of the reproduction number for seasonal, pandemic, and zoonotic influenza: a systematic review of the literature”. en. In: *BMC Infectious Diseases* 14.1 (Dec. 2014), p. 480. ISSN: 1471-2334. DOI: [10.1186/1471-2334-14-480](https://doi.org/10.1186/1471-2334-14-480).
- [5] Matteo Chinazzi et al. “The effect of travel restrictions on the spread of the 2019 novel coronavirus (COVID-19) outbreak”. In: *Science* 368.6489 (2020), pp. 395–400.
- [6] Laura Di Domenico et al. “Impact of lockdown on COVID-19 epidemic in Île-de-France and possible exit strategies”. In: *BMC medicine* 18 (2020), pp. 1–13.

- [7] S. Gonçalves, G. Abramson, and M. F. C. Gomes. “Oscillations in SIRS model with distributed delays”. en. In: *The European Physical Journal B* 81.3 (June 2011), pp. 363–371. ISSN: 1434-6028, 1434-6036. DOI: [10.1140/epjb/e2011-20054-9](https://doi.org/10.1140/epjb/e2011-20054-9).
- [8] Scott Greenhalgh and Carly Rozins. “A generalized differential equation compartmental model of infectious disease transmission”. en. In: *Infectious Disease Modelling* 6 (2021), pp. 1073–1091. ISSN: 24680427. DOI: [10.1016/j.idm.2021.08.007](https://doi.org/10.1016/j.idm.2021.08.007).
- [9] Claudius Gros. *Complex and Adaptive Dynamical Systems: A Comprehensive Introduction*. Springer Nature, 2024.
- [10] Herbert W. Hethcote, Harlan W. Stech, and P. Van Den Driessche. “Nonlinear Oscillations in Epidemic Models”. en. In: *SIAM Journal on Applied Mathematics* 40.1 (Feb. 1981), pp. 1–9. ISSN: 0036-1399, 1095-712X. DOI: [10.1137/0140001](https://doi.org/10.1137/0140001).
- [11] Paul Hurtado and Cameron Richards. “A procedure for deriving new ODE models: Using the generalized linear chain trick to incorporate phase-type distributed delay and dwell time assumptions”. en. In: *Mathematics in Applied Sciences and Engineering* 1.4 (Dec. 2020), pp. 410–422. ISSN: 2563-1926. DOI: [10.5206/mase/10857](https://doi.org/10.5206/mase/10857).
- [12] Paul J. Hurtado and Adam S. Kiro Singh. “Generalizations of the ‘Linear Chain Trick’: incorporating more flexible dwell time distributions into mean field ODE models”. en. In: *Journal of Mathematical Biology* 79.5 (Oct. 2019), pp. 1831–1883. ISSN: 0303-6812, 1432-1416. DOI: [10.1007/s00285-019-01412-w](https://doi.org/10.1007/s00285-019-01412-w).
- [13] Chun-Hsien Li, Chiung-Chiou Tsai, and Suh-Yuh Yang. “Analysis of epidemic spreading of an SIRS model in complex heterogeneous networks”. In: *Communications in Nonlinear Science and Numerical Simulation* 19.4 (2014), pp. 1042–1054.
- [14] Xiaoyue Liu et al. “The role of seasonality in the spread of COVID-19 pandemic”. In: *Environmental research* 195 (2021), p. 110874.
- [15] Micaela Elvira Martinez. “The calendar of epidemics: Seasonal cycles of infectious diseases”. In: *PLoS pathogens* 14.11 (2018), e1007327.
- [16] Daniel Henrik Nevermann and Claudius Gros. “Mapping dynamical systems with distributed time delays to sets of ordinary differential equations”. In: *Journal of Physics A: Mathematical and Theoretical* 56.34 (Aug. 2023), p. 345702. ISSN: 1751-8113, 1751-8121. DOI: [10.1088/1751-8121/acea06](https://doi.org/10.1088/1751-8121/acea06).
- [17] Tyler J Ripperger et al. “Orthogonal SARS-CoV-2 serological assays enable surveillance of low-prevalence communities and reveal durable humoral immunity”. In: *Immunity* 53.5 (2020), pp. 925–933.
- [18] Bulcsú Sándor et al. “Kick control: using the attracting states arising within the sensorimotor loop of self-organized robots as motor primitives”. In: *Frontiers in neurorobotics* 12 (2018), p. 40.

- [19] Joel Wagner et al. “Societal feedback induces complex and chaotic dynamics in endemic infectious diseases”. In: arXiv:2305.15427 (May 2023). arXiv:2305.15427 [physics, q-bio]. URL: <http://arxiv.org/abs/2305.15427>.

A. Two-step block delay kernel

The flexibility of the general immunity-time SIRS model introduced in Sec. 2.2 allows studying more complex immunity-time kernels. The next logical step in the evolution of block delay kernels is the introduction of a two-step kernel, that is

$$K(t) = \tilde{\Theta}_N^{(T_1, T_2)}(t) = \frac{1}{2} \left(\Theta_N^{(T_1)}(t) + \Theta_N^{(T_2)}(t) \right) \xrightarrow{N \rightarrow \infty} \begin{cases} 1, & \text{for } 0 \leq t \leq T_1 \\ 0.5, & \text{for } T_1 < t \leq T_2 \\ 0, & \text{else} \end{cases}, \quad (13)$$

in which N controls the width of the steps and T_1, T_2 control the loci of the two steps, where in the following we choose $T_1 = T/2$ and $T_2 = T$. The two-step kernel may also be written in terms of a series expansion of Erlang kernels, thereby implicitly specifying expansion coefficients c_m

$$\tilde{\Theta}_N^{(T/2, T)}(t) \equiv \tilde{\Theta}_N^{(T)} = \frac{T}{N} \left(\sum_{m=1}^{N/2} K_m^{(N, T)}(t) + \frac{1}{2} \sum_{m=N/2+1}^N K_m^{(N, T)}(t) \right).$$

For an illustration of the two-step kernel see Fig. 4. The corresponding SIRS model then reads

$$\begin{aligned} \dot{I} &= \beta I \left(1 - I - \sum_{m=1}^{N/2} R_m - \frac{1}{2} \sum_{m=N/2+1}^N R_m \right) - \rho I \\ \dot{R}_1 &= \rho I - \frac{N}{T} R_1 \\ \dot{R}_m &= \frac{N}{T} (R_{m-1} - R_m). \end{aligned} \quad (14)$$

A.1. Endemic state and the onset of oscillations

The non-oscillatory endemic state of the SIRS model (14) is again found at the root of the flow, which leads to

$$I_{\text{end}} = \frac{\beta - \rho}{\beta(1 + \frac{3}{4}\rho T)}.$$

As the step widths increase, i.e. as the order parameter N decreases, I_{end} loses stability in a Hopf bifurcation which leads to periodic oscillations. The onset of these endemic oscillations is again found by computing the root of the maximal eigenvalue’s real part

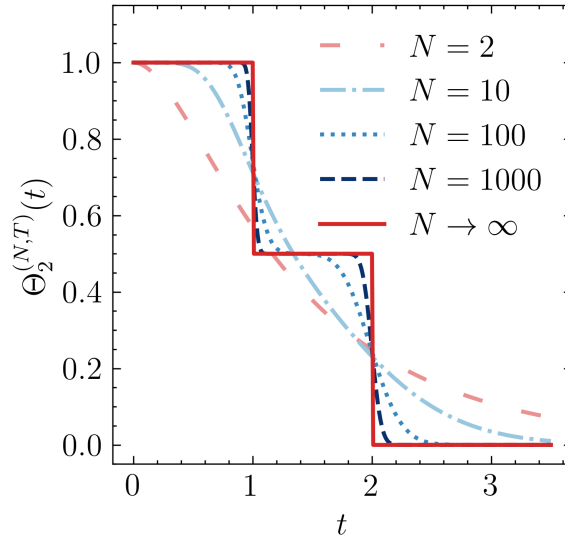


Figure 4: Two-step kernels $\tilde{\Theta}_N^{(T)}(t)$, as defined in (13), for $T = 2$ and different values of N . The double step results from a superposition of two step functions with time constants $T_1 = T/2$ and $T_2 = T$. For small $N = 2$, a quasi-exponential distribution is recovered.

of the Jacobian

$$\mathbf{J}|_{I_{\text{end}}} = \begin{pmatrix} -\frac{4(\beta-\rho)}{3\rho T+4} & \cdots & -\frac{2(\beta-\rho)}{3\rho T+4} & \cdots \\ \rho & -\frac{N}{T} & & \\ & \frac{N}{T} & -\frac{N}{T} & \\ & & \cdots & \ddots \end{pmatrix}.$$

Contrary to our expectations we could identify a second type of endemic oscillations, which arises independently of the Hopf bifurcation induced oscillations. For parameter values above the Hopf bifurcation curve we observe a small stable limit cycle in the phase space (I, R) triggered by the destabilization of the endemic state but also a second larger stable limit cycle, resembling severe periodic outbreaks with the period almost doubled compared to the Hopf induced limit cycle, see Fig. 6. Importantly, endemic oscillations persist below the Hopf bifurcation curve with the implication that the onset of oscillations lies below the Hopf bifurcation.

The full bifurcation diagram is shown in Fig. 5 (a). Compared to the model with single soft step kernel (12) (see Fig. 2), we find the locus of the Hopf bifurcation greatly shifted upwards. Consequently, destabilization of I_{end} , as well as the onset of Hopf bifurcation-induced oscillations, requires considerably larger immunity times $T \gtrsim 40$. Furthermore, the Hopf bifurcation curve is less steep which means that the destabilization of I_{end} generally requires larger N and thus sharper steps. These results seem plausible as the two-step kernel is closer to an exponential kernel than the block delay kernel, where in the exponential case no stable oscillations occur at all and I_{end} remains stable. On

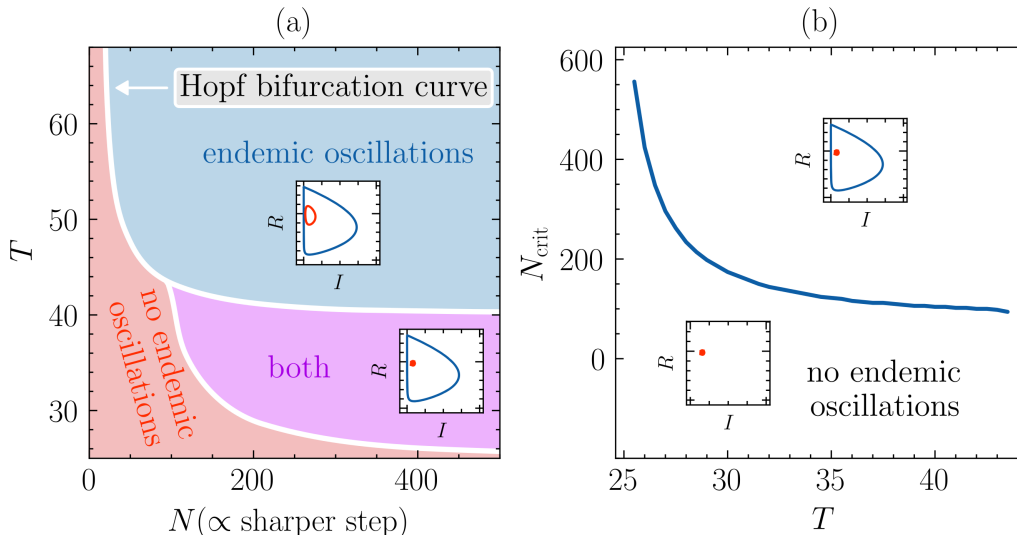


Figure 5: **(a)** Shows the full bifurcation diagram for the two-step kernel system (14) with $\beta = 2$ and $\rho = 1$. Parameter regions shaded in red lead to a decay of oscillations to the constant endemic state. In the purple shaded region we observe multistability, where the system either decays to I_{end} or enters endemic oscillations, depending on initial conditions. In the blue shaded region the system shows endemic oscillations for all (N, T) . The specific shape of the oscillations depends on the initial conditions. In **(b)** we present the critical values of the order parameter N_{crit} at which oscillations appear as a function of $T < T_{\text{Hopf}}$.

the other hand, unlike in the model (12) with a block delay kernel, endemic oscillations are present below the Hopf bifurcation curve. The asymptotic behavior of the system crucially depends on initial conditions. If the system is close to the fixpoint, the fraction of infected individuals will quickly converge to I_{end} , whereas severe periodic outbreaks may be observed even below the Hopf bifurcation if the system is further away from the fixpoint and importantly also for initial conditions resembling a few initial infections in an otherwise infection-naive population, see Fig. 6.

For $T < T_{\text{Hopf}}$ oscillations die out completely below a critical value of the order parameter N_{crit} . We find that N_{crit} diverges almost exponentially with increasing distance to the Hopf bifurcation curve, viz for shorter immunity times, oscillations only appear for sharp steps, see Fig. 5 (b). We find that in the limit $N \rightarrow \infty$ the potential for two limit cycles is retained.

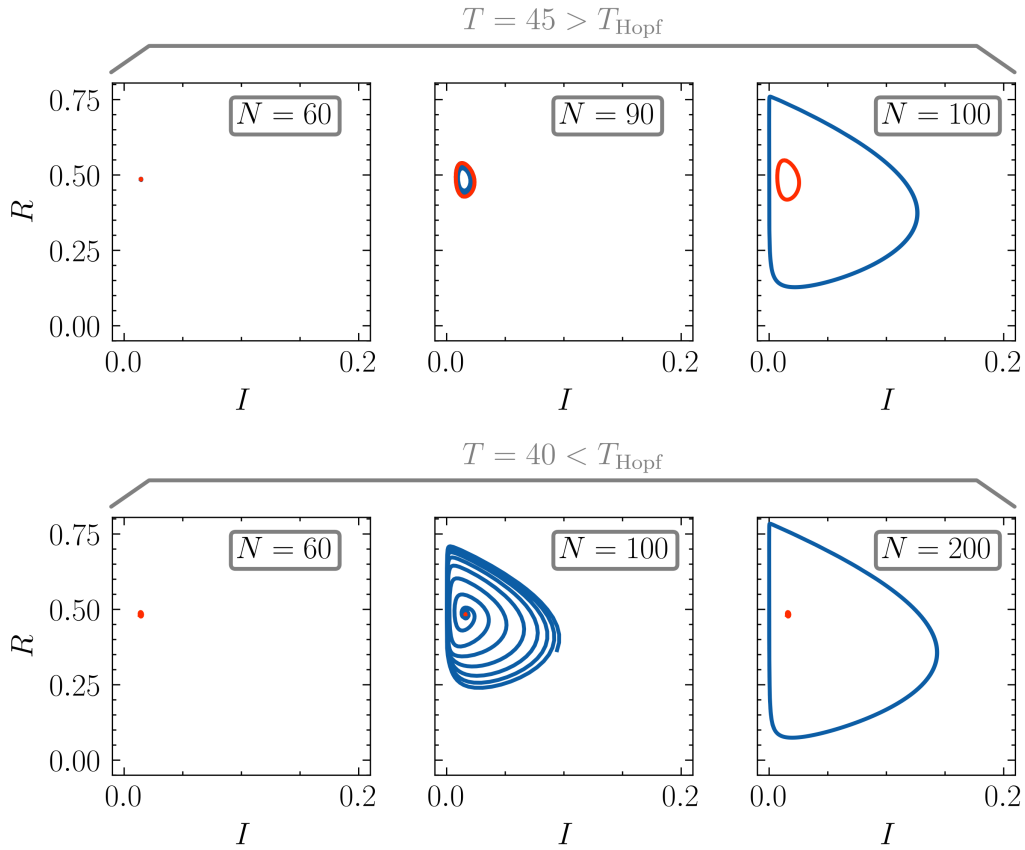


Figure 6: Phase space plots (I, R) for the two-step kernel system (14) with $\beta = 2$ and $\rho = 1$. The top row shows the dynamics above the Hopf bifurcation curve, the bottom row shows the dynamics below the Hopf bifurcation curve. Red trajectories were sampled using an initial condition close to the fixpoint, whereas blue trajectories were sampled using initial conditions resembling a few initial infections in an otherwise pathogen-naive population. Multistability observed in the two-step model is shown in the right-most column.